Stability of a dipolar BEC in a pancake potential using the Dini expansion Hankel transform

David Strachan and Edward Gandar

August 13, 2020

Contents

1 The Gross-Pitaevskii equation (GPE) for dipolar condensates in three dimensions

At ultra-low temperatures the properties of a dipolar condensate with N atoms, each of mass m, can be described by the GPE below.

$$i\hbar\frac{\partial\psi(\mathbf{r},t)}{\partial t} = \left[-\frac{\hbar^2}{2m}\nabla^2 + V_{ext}(\mathbf{r}) + \frac{4\pi\hbar^2 a_s N}{m}|\psi(\mathbf{r}',t)|^2 \right.$$
$$\left. + N\int_V U_{dd}(\mathbf{r}-\mathbf{r}')|\psi(\mathbf{r},t)|^2 d^3\mathbf{r}' \right]\psi(\mathbf{r},t) \quad (1.1)$$

where $\int_V d^3\mathbf{r}|\psi(\mathbf{r},t)|^2 = 1$ and a_s is the atomic s-wave scattering length. The trapping potential is assumed to be either in the form

$$V_{ext} = \frac{1}{2}m(w^2x^2 + w^2y^2 + w_z^2z^2)$$

and is assumed to have cylindrical symmetry about the z axis, or a circle box potential of radius R,

$$V_{ext}(r) = \begin{cases} 0 & \text{for } r < R \\ \infty & \text{otherwise} \end{cases}$$

and

$$V_{ext}(z) = \frac{1}{2}mw_z^2z^2$$

harmonic in the z axis. Where w is the angular frequency.

The dipolar interaction, for magnetic dipoles, is described by the equation:

$$U_{dd}(\mathbf{r}-\mathbf{r}') = \frac{\mu_0\bar{\mu}^2}{4\pi}\frac{1-3\cos^2(\theta)}{|\mathbf{r}-\mathbf{r}'|^3} \quad (1.2)$$

where θ is the angle between $\mathbf{r}-\mathbf{r}'$ and the direction of the polarization (chosen to be z) μ_0 is the permeability of free space, and $\bar{\mu}$ is the dipole moment of the atom.

In the case of the harmonic potential, we go into dimensionless units: $t \mapsto t_st, \mathbf{r} \mapsto x_s\mathbf{r}, \psi \mapsto \psi x_s^{-\frac{3}{2}}$, with $x_s = \sqrt{\frac{\hbar}{m\omega}}$ and $t_s = \omega = \min(w_x, w_y, w_z)$ we end up with the equation

$$i\frac{\partial\psi(\mathbf{r},t)}{\partial t} = \left[-\frac{1}{2}\nabla^2 + V_{trap} + g_s|\psi(\mathbf{r},t)|^2 \right.$$
$$\left. + D\int_V U_{3D}(\mathbf{r}-\mathbf{r}')|\psi(\mathbf{r}',t)|^2 d^3\mathbf{r}' \right]\psi(\mathbf{r},t) \quad (1.3)$$

where

$$V_{trap} = \frac{1}{2}(\gamma_x^2x^2 + \gamma_y^2y^2 + \gamma_z^2z^2) \quad (1.4)$$

and

$$U_{3D}(\mathbf{r}-\mathbf{r}') = \frac{1-3\cos^2(\theta)}{|\mathbf{r}-\mathbf{r}'|^3} \quad (1.5)$$

where $g_s = \frac{4\pi a_s N}{x_s}$, $\gamma_i = \frac{w_i}{w}$, $i = x, y, z$, is the trap ratio and $D = \frac{mN\mu_0\bar{\mu}^2}{4\pi\hbar^2 x_s}$.

Similarly in the case of the box potential, we go into dimensionless units, however the natural length and time scales are different Refs [1],[2],[3]. Namely, $x_s = L$ where L is a chosen fraction of the size (radius) of the box, and $t_s = \frac{mL^2}{\hbar}$. We thus end up with the equation

$$i\frac{\partial\psi(\mathbf{r},t)}{\partial t} = \left[-\frac{1}{2}\nabla^2 + V_{trap} + g_s^{box}|\psi(\mathbf{r},t)|^2 \right.$$
$$\left. + D^{box}\int_V U_{3D}(\mathbf{r}-\mathbf{r}')|\psi(\mathbf{r}',t)|^2 d^3\mathbf{r}' \right]\psi(\mathbf{r},t) \quad (1.6)$$

where

$$V_{trap}(r) = \begin{cases} 0 & \text{for } r < \Omega \\ \infty & \text{otherwise} \end{cases}$$

and

$$V_{trap}(z) = \frac{1}{2}\frac{m^2w_z^2L^4}{\hbar^2}z^2 \quad (1.7)$$

harmonic in the z axis.

where $g_s^{box} = \frac{4\pi Na_s}{L}$, $D^{box} = \frac{mN\mu_0\bar{\mu}^2}{4\pi\hbar^2 L}$ and $\Omega = \frac{R_{box}}{L}$. The reason for doing this instead of simply having $R_{box} = L$, where R_{box} is the radius if the trap is explained in section [INSERT SECTION NAME].

PLEASE CHECK IF THIS IS VALID

2 Evaluation of dipole interaction

The long-range anisotropic dipole potential is usually hard to calculate, however the integral is efficiently evaluated in Fourier space with the use of the convolution theorem Ref[4]. Recall the dipolar interaction term $\Phi_{dd}(\mathbf{r},t)$, stated again here as:

$$\Phi_{dd}(\mathbf{r},t) = \int_V d^3\mathbf{r}' U_{dd}(\mathbf{r}-\mathbf{r}')|\psi(\mathbf{r}',t)|^2 \quad (2.1)$$

The convolution theorem allows us to rewrite this as

$$\Phi_{dd}(\mathbf{r},t) = \mathcal{F}^{-1}[\tilde{U}_{dd}(\mathbf{k})\tilde{n}(\mathbf{k},t)] \quad (2.2)$$

where $\mathcal{F}$ ($\mathcal{F}^{-1}$) denotes the (inverse) Fourier transform, $\tilde{U}_{dd}(\mathbf{k}) = \mathcal{F}[U_{dd}(\mathbf{r})]$ is the k-space dipolar potential, and $\tilde{n}(\mathbf{k},t)$ is the density in k-space. The numerical calculation of this convolution is simply handled by the fast Fourier transforms (FFT) algorithms. However, since the FFT algorithms are naturally periodic, alias copies of the system can interact, by virtue of the long-range nature of the dipole interaction. In order to overcome this effect, we assume cylindrical symmetry of the system, which allows us to make use of a Hankel transform which does not assume periodicity, and thus doesn't produce alias copies. This also has the added benefit of reducing the number of effective dimensions from 3D (x,y,z), to 2D (r,z), which also greatly reduces computational time. (We will discuss this more in detail later in section 3). We also truncate the dipole potential in the z direciton to ensure that phantom copies cannot interact.

If the hankel transform is not used the standard truncated forms of the dipole term are the following. The first variant involves a spherical cut-off, which is used for almost-spherical sized systems (small γ_i). Restricting the range of the dipole interaction to a sphere of radius R_c, gives us the potential

$$U_{dd}^{R_c}(\mathbf{r} - \mathbf{r}') = \begin{cases} \frac{\mu_0 \bar{\mu}^2}{4\pi} \frac{1-3\cos^2(\theta)}{|\mathbf{r}-\mathbf{r}'|^3}, & \text{for } r < R_c \\ 0, & \text{otherwise} \end{cases} \quad (2.3)$$

As long as $R_c > R_{max}$ where R_{max} is the system size, this potential should reduce the effect of alias copies. The analytical Fourier transform is

$$\tilde{U}_{dd}(k) = \frac{C_{dd}}{3}\left[1+3\frac{\cos(R_c k)}{(R_c k)^2}-3\frac{\sin(R_c k)}{(R_c k)^3}\right](3\cos(\theta_k)^2-1) \quad (2.4)$$

This works for near-spherical traps, but if the system is highly oblate (if the trap is pancake like), the grid size in each dimension must still extend beyond R_{max}. This means the number of grid points in the tight direction required must be large to ensure sufficient resolution. A fix to this problem is to introduce a cylindrical cut-off to the dipole potential, given as

$$U_{dd}^{R_c}(\mathbf{r}-\mathbf{r}') = \begin{cases} \frac{\mu_0 \bar{\mu}^2}{4\pi} \frac{1-3\cos^2(\theta)}{|\mathbf{r}-\mathbf{r}'|^3}, & \text{for } \rho < \rho_c \text{ and } |z| < Z_c \\ 0, & \text{otherwise} \end{cases} \quad (2.5)$$

The Fourier transform is semi-analytic [4]

$$\tilde{U}_{dd}(\mathbf{k}) = \frac{C_{dd}}{3}(3\cos\theta_k{}^2 - 1)$$
$$+ C_{dd}e^{-Z_c k_\rho}[\sin\theta_k{}^2\cos Z_c k_z - \sin\theta_k\cos\theta_k\sin Z_c k_z]$$
$$- C_{dd}\int_{\rho_c}^{\infty}\rho d\rho\int_0^{Z_c}dz\cos k_z z\frac{\rho^2-2z^2}{(\rho^2+z^2)^{\frac{5}{2}}}J_0(k_\rho\rho), \quad (2.6)$$

Where J_0 is the zeroth order Bessel function of the first kind.

The final line cannot be done analytically, but requires numerical integration, which is computationally costly but only required once per simulation set-up. However, if the integral is not calculated, the first two terms act as a dipole interaction truncated in the z direction only Ref[5]. We use this form of the dipole potential, since the use of the Hankel transform in the ρ direction does not produce alias copies and thus does not need to be truncated. The Hankel transform is discussed in more detail in the next section.

3 Hankel Transform using the Dini expansion

If the dipole polarization is along the z axis, the ground state will be cylindrically symmetric in a harmonic trap (or circular box potential). This can reduce a 3D system to an effective 2D system, where

only the r and z coordinates are needed. If we are in cylindrical coordinates, the space where the r component of the Laplacian operator is diagonalised is bessel space (more specifically zeroth order bessel functions of the first kind). To transform from position space to bessel space, we use a Hankel transform. In ref [6] they outline a very efficient method to compute a discrete Hankel transform for a finite range of r. First, we rewrite the function in both position space $f(r)$ and bessel space $g(\rho)$ as a Dini series.

If $0 < r < b$ and $0 < \rho < \beta$ then we can write f(r) and $g(\rho)$ as

$$f(r) = \frac{2}{b^2}\sum_{n=0}^{\infty}f_n J_0^{-2}(\alpha_n)J_0(\frac{\alpha_n r}{b}) \quad (3.1)$$

$$g(\rho) = \frac{2}{\beta^2}\sum_{n=0}^{\infty}g_n J_0^{-2}(\alpha_n)J_0(\frac{\alpha_n \rho}{\beta}) \quad (3.2)$$

where

$$f_n = \int_0^b rf(r)J_0(\frac{\alpha_n r}{b})dr = \frac{1}{2\pi}g(\frac{\alpha_n}{2\pi b}) \quad (3.3)$$

and

$$g_n = \int_0^\beta \rho g(\rho)J_0(\frac{\alpha_n \rho}{\beta})d\rho = \frac{1}{2\pi}f(\frac{\alpha_n}{2\pi \beta}) \quad (3.4)$$

where α_n are the real nonnegative roots of the derivative of the zero-order Bessel function, $\alpha_0 = 0$. We can truncate these infinite sums to finite ones by using the fact that if $\alpha_N = S$ where $S = 2\pi b\beta$, both f_n and g_N are zero for $n > N$.

Defining a change of variables,

$$G(m) = g(\frac{\alpha_m}{2\pi b})|J_0^{-1}(\alpha_m)|\beta \quad (3.5)$$

$$F(n) = f(\frac{\alpha_n}{2\pi \beta})|J_0^{-1}(\alpha_n)|b \quad (3.6)$$

leads to the following formula for the discrete Hankel transform and its inverse,

$$G(m) = \sum_{n=0}^{N}c_{mn}F(n) \quad (3.7)$$

$$F(n) = \sum_{m=0}^{N}c_{nm}G(m) \quad (3.8)$$

where c_{nm} are the elements of a transform matrix,

$$c_{nm} = \frac{2}{S}|J_0^{-1}(\alpha_n)||J_0^{-1}(\alpha_m)|J_0(\frac{\alpha_n \alpha_m}{S}) \quad (3.9)$$

For this to hold, the matrix C has to satisfy $CC = I$, and C is a function of S only so S must be chosen correctly. In [6] they state that the optimum choice is

$$S = 2|J_0^{-1}(\alpha_k)|\sqrt{(1 + \sum_{n=1}^{N}J_0^{-2}(\alpha_n)J_0^2(\frac{\alpha_k \alpha_n}{J_{N+1}}))} \quad (3.10)$$

where

$$k = Int(\frac{N}{4}) \qquad (3.11)$$

Despite redefining S in a different way, as long as $S < \alpha_{N+1}$, this approach is still valid.

Further efficiency can be achieved by realising all solutions will be symmetric in z, so only $z \geqslant 0$ is needed. Instead of using a Fourier transform we can use a fast cosine transform, which leads to faster computational time overall.

4 Extending the Hankel Transform to the non-symmetric case

I'll outline this separately to the symmetric case, but it's just the general case so includes the above transform that we use for the code.

It isn't only the fact it can reduce the dimensions of the problem that makes the Hankel transform useful, but it needs no assumption of periodicity unlike the fourier transform, meaning no cut off is needed. The reason for this being such an advantage is that the integral in Eq 2.6 is quite computationally costly, and depends on various parameters meaning this integral may have to be repeatedly calculated if any of these parameters change. So, even in the non-symmetric case, an extension to the method outlined in ref [6] which doesn't assume symmetry would be very useful. The Dini series is based on the Robin boundary condition where if the following is true,

$$b f'(b) + c_r f(b) = 0, \qquad (4.1)$$

where c_r is a constant, then a function f(r) defined for $r \geqslant 0$ can be expressed as

$$f(r) = \frac{2}{b^2} \sum_{n=0}^{\infty} f_n J_\nu^{-2}(\lambda_{\nu,n}) J_\nu(\lambda_{\nu,n} r/b) \qquad (4.2)$$

where $\lambda_{\nu,n}$ is the nth root of

$$r J'_\nu(r) + c_{r,\rho} J_\nu(r) = 0. \qquad (4.3)$$

The coefficients f_n are given by

$$f_n = \frac{\lambda_{\nu,n}^2}{c_r^2 + \lambda_{\nu,n}^2 - \nu^2} \int_0^b r f(r) J_\nu(\lambda_{\nu,n} r/b) dr$$

$$= \frac{\lambda_{\nu,n}^2}{2\pi(c_r^2 + \lambda_{\nu,n}^2 - \nu^2)} \mathcal{F}_\nu(\lambda_{\nu,n}/2\pi b) \quad (4.4)$$

$\mathcal{F}_\nu(\rho)$ represents the function f(r) in ν^{th} order bessel space. As this is also defined for $\rho \geqslant 0$, the following is also true

$$\mathcal{F}_\nu(\rho) = \frac{2}{\beta_\nu^2} \sum_{n=0}^{\infty} g_n J_\nu^{-2}(\lambda_{\nu,n}) J_\nu(\lambda_{\nu,n} \rho/\beta_\nu) \qquad (4.5)$$

given

$$\beta_\nu \mathcal{F}'_\nu(\beta_\nu) + c_\rho \mathcal{F}_\nu(\beta_\nu) = 0, \qquad (4.6)$$

The coefficients g_n are given by

$$g_n = \frac{\lambda_{\nu,n}^2}{c_\rho^2 + \lambda_{\nu,n}^2 - \nu^2} \int_0^{\beta_\nu} \rho \mathcal{F}_\nu(\rho) J_\nu(\lambda_{\nu,n} \rho/\beta_\nu) d\rho$$

$$= \frac{\lambda_{\nu,n}^2}{2\pi(c_\rho^2 + \lambda_{\nu,n}^2 - \nu^2)} f(\lambda_{\nu,n}/2\pi\beta_\nu) \quad (4.7)$$

Technically $\lambda_{\nu,n}$ has to be defined differently for (4.5) and (4.7) if $c_\rho \neq c_r$, but as we will see this is never the case. There are two main differences in the structure of this for a general $\nu \in \mathbb{Z}^+$ compared to the $\nu = 0$ case. The first and main problem is the potential for asymptotes if

$$c_{r,\rho}^2 + \lambda_{\nu,n}^2 = \nu^2, \qquad (4.8)$$

bearing mind that $\lambda_{\nu,n}$ takes many values and there is nothing preventing Eq 4.8 being true. We can easily get past this by realising that the choice of $c_{r,\rho}$ is arbitary. $c_{r,\rho}$ is(are) based on the Robin boundary condition, and because our system is bounded,

$$f(r \geqslant b) = 0 \qquad (4.9)$$

$$\mathcal{F}_\nu(\rho \geqslant \beta_\nu) = 0. \qquad (4.10)$$

Then, the only condition for (4.1) and (4.6) to hold is

$$\mathcal{F}'_\nu(\beta_\nu) = 0 = f'(b). \qquad (4.11)$$

and this is independent of $c_{r,\rho}$. The validity of (4.11) comes from the fact that as $f(x) \Rightarrow 0$, $f'(x) \Rightarrow 0$ provided both of these are smooth and continuous. I'm pretty sure this is true, otherwise the probability current would be non zero at the boundary so probability wouldn't be conserved. If, for any given ν we set $c_r = c_\rho = \nu$ this asymptotic behaviour no longer appears. This also leads to a simplifed expression as $\lambda_{\nu,n}^2$ cancels. This choice leads to the second difference, which is the nature of the roots $\lambda_{\nu,n}$. Inserting this value of c into Eq (4.3) leads to

$$r J'_\nu(r) + \nu J_\nu(r) = 0. \qquad (4.12)$$

($c = -\nu$ also works, which might cause problems if it leads to different solutions, I haven't checked this). Using the following recurrence relations for Bessel functions,

$$J_{\nu-1}(z) - J_{\nu+1}(z) = 2 J'_\nu(z), \qquad (4.13)$$

$$J_{\nu-1}(z) + J_{\nu+1}(z) = \frac{2\nu}{z} J_\nu(z), \qquad (4.14)$$

Eq (4.12) simplifies to

$$2\nu J_\nu(r) - r J_{\nu-1}(r) = 0. \qquad (4.15)$$

This has to be solved numerically, but it's essentially equating two Bessel functions of adjacent order so we could write a function which takes the two bessel functions as arrays (with the 2ν and r prefactors) and then takes one away from the other. The output would be an array of the r values when they're equal, which probably doesn't take long at all. Further to this, for a given ν this only has to be calculated once

as it doesn't depend on any parameters of our system apart from the number of data points in our r array, which will be the number of roots we need. But again, a large number N_{max} can be calculated so even if N is changed, provided $N < N_{max}$ the roots won't have to be recalculated.

4.1 The Form of the General Hankel Transform

If $\lambda_{\nu,N} = S$ where $S_\nu = 2\pi b\beta_\nu$, both f_n and g_n are zero for $n > N$. Defining a change of variables, (I realise this notation is poor because I've already used $\mathcal{F}_\nu$ to define f in bessel space, I can change this)

$$G_\nu(m) = \mathcal{F}_\nu(\frac{\lambda_{\nu,m}}{2\pi b})|J_\nu^{-1}(\lambda_{\nu,m})|\beta_\nu \qquad (4.16)$$

$$F_\nu(n) = f(\frac{\lambda_{\nu,n}}{2\pi \beta_\nu})|J_\nu^{-1}(\lambda_{\nu,n})|b \qquad (4.17)$$

leads to the formula for the general, discrete Hankel transform and its inverse for any $\nu \in \mathbb{Z}^+$,

$$G_\nu(m) = \sum_{n=0}^{N} C_{\nu,mn} F_\nu(n) \qquad (4.18)$$

$$F_\nu(n) = \sum_{n=0}^{N} C_{\nu,nm} G_\nu(m) \qquad (4.19)$$

where $C_{\nu,nm}$ are the elements of a transform matrix,

$$C_{\nu,nm} = \frac{2}{S_\nu}|J_\nu^{-1}(\lambda_{\nu,n})||J_\nu^{-1}(\lambda_{\nu,m})|J_\nu(\frac{\lambda_{\nu,n}\lambda_{\nu,m}}{S_\nu}) \qquad (4.20)$$

For this to hold, the matrix C has to satisfy $CC = I$, and C is a function of S only so S must be chosen correctly. This can be done numerically by varying S until $det[CC^T] - 1 = 0$, or by a more analytical approach. In the next section a semi-analytical solution is proposed. $S_\nu = \lambda_{\nu,N+1}$ will give enough accuracy for most simulations, as stated in ref[INSERT REFERENCE], although their structure is slightly different.

4.2 Finding the optimal value for S_ν

One way to define an orthogonal matrix is $det[C] = \pm 1$. One problem with using this definition is that the expression for the determinant of an N by N matrix isn't very nice. Another, more useful definition we can use is the fact that the columns or rows form an orthonormal basis, so if C_ν is orthogonal then

$$C_{\nu,i} \cdot C_{\nu,j} = \delta_{ij}. \qquad (4.21)$$

I will only refer to columns as C_ν is symmetric, so anything that is true for its columns is true for its rows. Choosing two specific values for i and j, we can solve

$$C_{\nu,n}(S_\nu) \cdot C_{\nu,m}(S_\nu) = \delta_{nm}, \qquad (4.22)$$

for $S_\nu(n,m)$. Now if there exists an exact solution to 4.21, where

$$C_{\nu,i}(S_{opt,\nu}) \cdot C_{\nu,j}(S_{opt,\nu}) = \delta_{ij}, \qquad (4.23)$$

then this solution, $S_{opt,\nu}$, will be independent of any specific values of i and j. However, if both solution spaces for 4.21 and 4.22 are singular, then

$$S_\nu(n,m) = S_{opt,\nu}. \qquad (4.24)$$

So as long as this holds, S_ν will be independent of n and m. This means that we can choose any two columns and solve 4.22 for S_ν giving an orthogonal transformation matrix $C_\nu(S_\nu)$, provided both 4.21 and 4.22 are singular. First, to solve 4.22 we separate the n=m case.

$$\frac{S_\nu^2 J_\nu^2(\lambda_{\nu,k})}{4} = \sum_{i=0}^{N} J_\nu^{-2}(\lambda_{\nu,i}) J_\nu^2\left(\frac{\lambda_{\nu,k}\lambda_{\nu,i}}{S_\nu}\right), \quad (4.25)$$

$$\frac{4}{S_\nu^2}|J_\nu^{-1}(\lambda_{\nu,n})||J_\nu^{-1}(\lambda_{\nu,m})|$$
$$\cdot \sum_{i=0}^{N} J_\nu^{-2}(\lambda_{\nu,i}) J_\nu\left(\frac{\lambda_{\nu,n}\lambda_{\nu,i}}{S_\nu}\right) J_\nu\left(\frac{\lambda_{\nu,m}\lambda_{\nu,i}}{S_\nu}\right) = 0,$$
$$(n,m,k = 0,1,2,...,N), \quad (4.26)$$

where $n \neq m$ and 4.25 is the $n = m$ case. These are implicit equations for S_ν, but S_ν can be extracted from within the argument of the bessel functions by employing a taylor expansion. Note that this the solution will no longer be exact as we are neglecting higher order terms. $\lambda_{\nu,N} < S_\nu < \lambda_{\nu,N+1}$ so we could taylor expand around $\lambda_{\nu,N}$ or $\lambda_{\nu,N+1}$. Due to the $\frac{1}{S_\nu^2}$ expression in 4.26, it seems sensible that S_ν would be closer to $\lambda_{\nu,N+1}$. Going to first order gives the following,

$$J_\nu\left(\frac{\lambda_{\nu,p}\lambda_{\nu,i}}{S_\nu}\right) = J_\nu\left(\frac{\lambda_{\nu,p}\lambda_{\nu,i}}{\lambda_{\nu,N+1}}\right) + \frac{\lambda_{\nu,p}\lambda_{\nu,i}}{\lambda_{\nu,N+1}^2} J_\nu'\left(\frac{\lambda_{\nu,p}\lambda_{\nu,i}}{\lambda_{\nu,N+1}}\right)\delta + ... \qquad (4.27)$$

where $\delta = \lambda_{\nu,N+1} - S_\nu$. Substituting 4.27 into 4.25 and 4.26 and rearranging gives

$$\frac{S_\nu^2 J_\nu^2(\lambda_{\nu,k})}{4} = \Sigma_1 + \frac{2\lambda_{\nu,k}\delta}{\lambda_{\nu,N+1}^2}\Sigma_2, \qquad (4.28)$$

$$\frac{4}{S_\nu^2}|J_\nu^{-1}(\lambda_{\nu,n})||J_\nu^{-1}(\lambda_{\nu,m})|\left[\Sigma_3 + \frac{\delta}{\lambda_{\nu,N+1}^2}\Sigma_4\right] = 0, \qquad (4.29)$$

respectively, where

$$\Sigma_1 = \sum_{i=0}^{N} J_\nu^{-2}(\lambda_{\nu,i}) J_\nu^2\left(\frac{\lambda_{\nu,k}\lambda_{\nu,i}}{\lambda_{\nu,N+1}}\right),$$

$$\Sigma_2 = \sum_{i=0}^{N} \lambda_{\nu,i} J_\nu^{-2}(\lambda_{\nu,i}) J_\nu\left(\frac{\lambda_{\nu,k}\lambda_{\nu,i}}{\lambda_{\nu,N+1}}\right) J_\nu'\left(\frac{\lambda_{\nu,k}\lambda_{\nu,i}}{\lambda_{\nu,N+1}}\right),$$

$$\Sigma_3 = \sum_{i=0}^{N} J_\nu^{-2}(\lambda_{\nu,i}) J_\nu\left(\frac{\lambda_{\nu,n}\lambda_{\nu,i}}{\lambda_{\nu,N+1}}\right) J_\nu\left(\frac{\lambda_{\nu,m}\lambda_{\nu,i}}{\lambda_{\nu,N+1}}\right),$$

$$\Sigma_4 = \sum_{i=0}^{N} J_\nu^{-2}(\lambda_{\nu,i})\lambda_{\nu,i}\left[\lambda_{\nu,m} J_\nu\left(\frac{\lambda_{\nu,n}\lambda_{\nu,i}}{\lambda_{\nu,N+1}}\right) J_\nu'\left(\frac{\lambda_{\nu,m}\lambda_{\nu,i}}{\lambda_{\nu,N+1}}\right) \right.$$
$$\left. + \lambda_{\nu,n} J_\nu\left(\frac{\lambda_{\nu,m}\lambda_{\nu,i}}{\lambda_{\nu,N+1}}\right) J_\nu'\left(\frac{\lambda_{\nu,n}\lambda_{\nu,i}}{\lambda_{\nu,N+1}}\right)\right]. \qquad (4.30)$$

Eq 4.28 is a quadratic in S_ν and gives the following solution,

$$S_{u,\nu} = \frac{4\lambda_{\nu,k}\Sigma_2}{\lambda_{\nu,N+1}^2 J_\nu^2(\lambda_{\nu,k})}$$
$$\cdot\left[-1+\lambda_{\nu,N+1}\sqrt{1+\frac{\lambda_{\nu,N+1}J_\nu^2(\lambda_{\nu,k})}{2\lambda_{\nu,k}\Sigma_2}\left(1+\frac{\lambda_{\nu,N+1}}{2\lambda_{\nu,k}\Sigma_2}\Sigma_1\right)}\right],$$
$$(4.31)$$

where the positive root has been taken as $S_\nu > 0$. 4.29 can be solved by setting the expression inside the brackets to zero, which gives,

$$S_{o,\nu} = \lambda_{\nu,N+1}\left(1+\lambda_{\nu,N+1}\frac{\Sigma_3}{\Sigma_4}\right). \qquad (4.32)$$

If $S_\nu = S_{o,\nu}$, all the columns and rows of C_ν will be (approximately) orthogonal. If $S_\nu = S_{u,\nu}$, all the columns and rows of C_ν will (approximately) have magnitude 1. The reason for this approximate solution comes from the finite Taylor expansion used, as the true solution will be when an infinite Taylor expansion is used. When the taylor expansion is first order only, both 4.31 and 4.32 are singular for a given n,m or k, so they must be (approximately) equal. If a higher order Taylor expansion was used, 4.31 and 4.32 may have multiple solutions for $\lambda_{\nu,N} < S_\nu < \lambda_{\nu,N+1}$, as they will be higher degree polynomials. If the solutions stayed singular within $\lambda_{\nu,N} < S_\nu < \lambda_{\nu,N+1}$, then

$$\lim_{\beta\to\infty} S_{o,\nu} = \lim_{\beta\to\infty} S_{u,\nu} = S_{opt,\nu}, \qquad (4.33)$$

where β represents the order of the taylor expansion used, and $S_{opt,\nu}$ is the exact solution of 4.23. If we use a first order Taylor expansion only, expressions 4.31 and 4.32 will vary slightly for different values of n,m and k. These differences will be very small due to $\delta/\lambda_{\nu,N+1} \ll 1$. So, even for $\beta = 1$,

$$S_{u,\nu} \approx S_{o,\nu} \approx S_{opt,\nu}. \qquad (4.34)$$

4.3 Application to the Split Step Method

The way in which this transform is useful within the split step method is in diagonalising the laplacian operator. In cylindrical coordinates, the laplacian operator, $\mathcal{L}\{\psi\} = \nabla^2\psi(r,\theta,z)$ can be rewritten as

$$\mathcal{L}\{\psi\} = \frac{1}{r}\frac{\partial}{\partial r}\left(r\frac{\partial\psi}{\partial r}\right) + \frac{1}{r^2}\frac{\partial^2\psi}{\partial\theta^2} + \frac{\partial^2\psi}{\partial z^2}. \qquad (4.35)$$

By taking the separable ansatz in the form

$$\psi(r,\theta,z) = R(r)\Theta(\theta)Z(z) \qquad (4.36)$$

and applying the operator gives

$$\frac{\mathcal{L}\{\psi(r,\theta,z)\}}{\psi(r,\theta,z)} = \frac{1}{rR}\frac{\partial}{\partial r}\left(r\frac{\partial R}{\partial r}\right) + \frac{1}{r^2\Theta}\frac{\partial^2\Theta}{\partial\theta^2} + \frac{1}{Z}\frac{\partial^2 Z}{\partial z^2}. \qquad (4.37)$$

The space where the RHS of 4.23 is constant is where $\mathcal{L}\{\psi\}$ is diagonal. As the second term is the only one which includes an angular component, it must be a constant function. I.e,

$$\frac{1}{\Theta}\frac{d^2\Theta}{d\theta^2} = -\nu^2, \qquad (4.38)$$

where $\nu \in \mathbb{Z}^+$ to satisfy the condition $\Theta(\theta + 2n\pi) = \Theta(\theta), n \in \mathbb{Z}$. This gives oscillatory solutions and is diagonalised in fourier space. for a specific ν, 4.23 becomes

$$\frac{\mathcal{L}_\nu\{\psi\}}{\psi} = \mathcal{R}\{R\} + \mathcal{Z}\{Z\} \qquad (4.39)$$

where

$$\mathcal{R}_\nu\{R\} = \frac{1}{rR}\frac{\partial}{\partial r}\left(r\frac{\partial R}{\partial r}\right) - \frac{\nu^2}{r^2} \qquad (4.40)$$

and

$$\mathcal{Z}\{Z\} = \frac{1}{Z}\frac{\partial^2 Z}{\partial z^2}. \qquad (4.41)$$

The space of functions that make 4.26 and 4.27 constant are

$$\mathcal{R}_\nu\{J_\nu(k_r r)\} = -k_r^2, \qquad (4.42)$$
$$\mathcal{Z}\{e^{ik_z z}\} = -k_z^2, \qquad (4.43)$$

So, for a given $\nu = \nu_0$,

$$\mathcal{L}_{\nu_0}\{\psi(\mathbf{r})\} \Rightarrow -(k_z^2 + k_r^2)\psi(\mathbf{k}, \nu = \nu_0) \qquad (4.44)$$

where $\psi(\mathbf{k}, \nu = \nu_0) = \mathcal{F}_z\mathcal{H}_{\nu_0}\{\psi(\mathbf{r})\}$. Obviously, this isn't the full laplacian as it's only diagonalising $\mathcal{L}$ for a specific 'slice' of ν. In this structure, to fully diagonalise $\mathcal{L}_{3D}$ a fourier transform must be applied in both the θ and z direction. Then a different discrete Hankel transform 4.19 must be applied for each 'slice' of ν along the r direction to arrive at the correct Bessel space. In this range of frequency spaces, each $\mathcal{L}_\nu$ will be diagonal along the k_r and k_z directions, with the laplacian already diagonalised along the ν direction.

This seems to make things very complicated as hundreds of different ν's and thus different versions of the Hankel transform would be needed. However, this wouldn't add any computational cost when running the code, because despite a different Hankel transform being called each time they each take the same computational time. The only real complication would be calculating each different C matrix and S value for every ν, and the corresponding roots of eq(4.15) needed. The parameters these depend on are b and N (providing this is true for the optimal value of S, which we haven't calculated yet). So whenever these parameters are changed, a considerable amount of code would have to be run but these are rarely changed and the code probably wouldn't take that long anyway. No cut off will be needed for θ, as despite needing periodicity for the fourier transform, this wouldn't be an approximation because the wave function will be periodic in θ by necessity. This means we can just use a cut off in the z direction, reducing the computational cost of this step.

5 Convergence using imaginary time propagation and the split step Fourier/Hankel method

There are many different methods to solve the GPE, and in this paper we make use of imaginary time propagation. The general procedure is shown below (Ref [7]). Consider the wavefunction $\Psi(\mathbf{r}, t)$ as a superposition of energy eigenstates $\psi_n(\mathbf{r})$ with eigenenergy E_n. We write

$$\Psi(\mathbf{r}, t) = \sum_n \psi_n(\mathbf{r}) e^{-iE_n t/\hbar} \qquad (5.1)$$

where $E_n > E_{n-1}$. Peform a Wick rotation $t \mapsto -i\tau$, so we have

$$\Psi(\mathbf{r}, -i\tau) = \sum_n \psi_n(\mathbf{r}) e^{-E_n \tau/\hbar} \qquad (5.2)$$

Clearly, the eigenenergy governs the decay rate, where eigenstates with higher eigenenergies decay faster. Thus by taking an approximation of the initial profile of the wavefunction, during propagation in imaginary time the excited states will dissipate, leaving behind the ground state. Note that since the ground state also decays, it is important to renormalise appropriately each iteration.

In order to propagate our wavefunction in (imaginary) time, we use the split-step Fourier/Hankel method Ref [8],[9]. We first write the GPE as

$$i\hbar \frac{\partial \psi(\mathbf{r}, t)}{\partial t} = \hat{H} \psi(\mathbf{r}, t) \qquad (5.3)$$

with $\hat{H}$ as the Hamiltonian of the system. We then decompose the Hamiltonian as $\hat{H} = \hat{T} + \hat{V}$ where $\hat{T} = -\hbar^2 \nabla^2/(2m)$ and $\hat{V} = V_{trap} + g|\psi|^2 + \Phi_{dd}$. Integrating from t to $t + \Delta t$ leads to

$$\psi(\mathbf{r}, t + \Delta t) = e^{-i\Delta t \hat{H}/\hbar} \psi(\mathbf{r}, t) \qquad (5.4)$$

Note that the operators $\hat{T}$ and $\hat{V}$ do not commute, hence $e^{-i\Delta t \hat{H}/\hbar} \neq e^{-i\Delta t \hat{T}/\hbar} e^{-i\Delta t \hat{V}/\hbar}$. However, we can make use of the approximation,

$$e^{-i\Delta t \hat{H}/\hbar} \approx e^{-i\Delta t \hat{V}/2\hbar} e^{-i\Delta t \hat{T}/\hbar} e^{-i\Delta t \hat{V}/2\hbar} \qquad (5.5)$$

Note that we can also equally apply $\hat{T}/2$, then $\hat{V}$ then $\hat{T}/2$. This approximation holds with error $\mathcal{O}(\Delta t^3)$ [10].

In position space $\hat{V}$ is diagonal, so the operation $e^{-i\Delta t \hat{H}/\hbar} \approx e^{-i\Delta t \hat{V}/2\hbar} \psi$ just corresponds to multiplication of $\psi(\mathbf{r}, t)$ by $e^{-i\Delta t \hat{H}/\hbar} \approx e^{-i\Delta t \hat{V}/2\hbar}$. Although $\hat{T}$ is not diagonal in position space, it becomes diagonal in momentum space, which can be done by taking the Fourier transform $\mathcal{F}$ of ψ, then multiplying by the kinetic energy operator in momentum space of $\tilde{\psi}(\mathbf{k}, t)$ with $e^{-i\hbar \Delta t k^2/2m}$.

Computationally, we repeat this process until the desired solution has been found within an appropriate tolerance.

6 Quasi 2D approach

When the axial trap is very strong, a good approximation to make is that the BEC in the axial direction is confined to the axial ground state Ref[11]

$$\phi(z) = \frac{1}{(\pi\epsilon)^{\frac{1}{4}}} e^{\frac{-z^2}{2\epsilon}}, \epsilon = \frac{1}{\gamma} \qquad (6.1)$$

We then take the ansatz

$$\psi(r, z) = \psi_{2D}(\mathbf{x}_\perp)\phi(z), \qquad (6.2)$$

and inserting this into Eq(3), multiplying by $\phi(z)$ and integrating over z we get the the following quasi 2D GPE

$$i\frac{\partial \psi_{2D}(\mathbf{x}_\perp, t)}{\partial t} = \Bigg[-\frac{1}{2}\nabla^2_{\mathbf{x}_\perp} + \frac{1}{2}(x^2 + y^2)$$
$$+ \frac{g_s}{\sqrt{2\pi\epsilon}}|\psi_{2D}(\mathbf{x}_\perp, t)|^2 + \frac{4\pi D}{3}$$
$$\cdot \int d\mathbf{k}_{x_\perp} e^{-2\pi i \mathbf{k}_{x_\perp} \cdot \mathbf{x}_\perp} \tilde{n}(\mathbf{k}_{x_\perp}, t) h_{2D}(\xi) \Bigg] \psi_{2D}(\mathbf{x}_\perp, t),$$
$$(6.3)$$

where

$$\tilde{n}(\mathbf{k}_{x_\perp}, t) = \int d\mathbf{x}_\perp e^{2\pi i \mathbf{k}_{x_\perp} \cdot \mathbf{x}_\perp} |\psi_{2D}(\mathbf{x}_\perp, t)|^2, \quad (6.4)$$

$$h_{2D}(\xi) = \frac{1}{\sqrt{2\pi\epsilon}}[2 - 3\sqrt{\pi} exp(\xi^2) erfc(\xi)], \quad (6.5)$$

$$\xi = k_{x_\perp} \sqrt{\frac{\epsilon}{2}}. \qquad (6.6)$$

This is very similar to the orginal GPE in structure, the only difference being the reduced dimension and the modified terms. We have assumed cylindrical symmetry so a Hankel transform can be used, reducing a 3D problem to a 1D one.

This method achieves very accurate results of within 0.001% of the true ground state with no interactions.
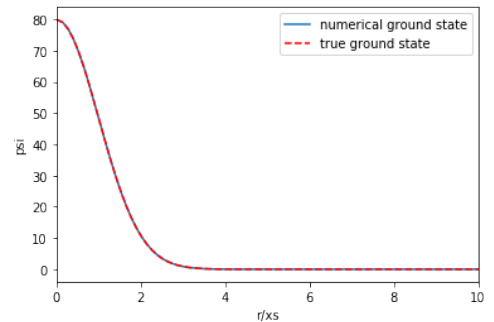

Figure 1: Comparison of the harmonic ground state and the numerical solution using the Quasi 2D Method

7 Accuracy with no interactions

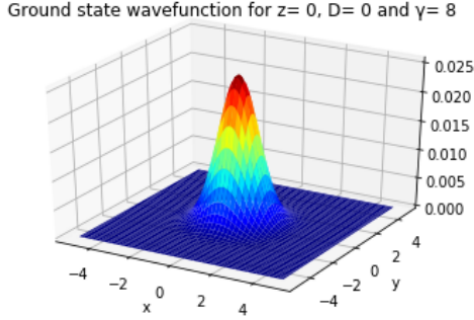In 3D, the ground state wavefunction with no interactions is shown below:

Figure 2: Ground state with $\gamma = 8$

In 3D using a hankel transform and a cosine fast transform, we achieve the same ground state within 0.008% of the true ground state with no interactions.
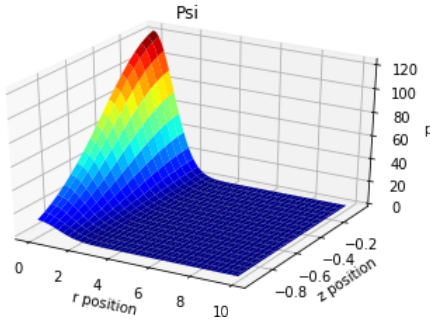

Figure 3: Ground state with $\gamma = 5$ using the Hankel transform and cosine transform

Using the Hankel transform in 2D (1D computationally), we achieve very accurate results compared to the harmonic oscillator ground state.
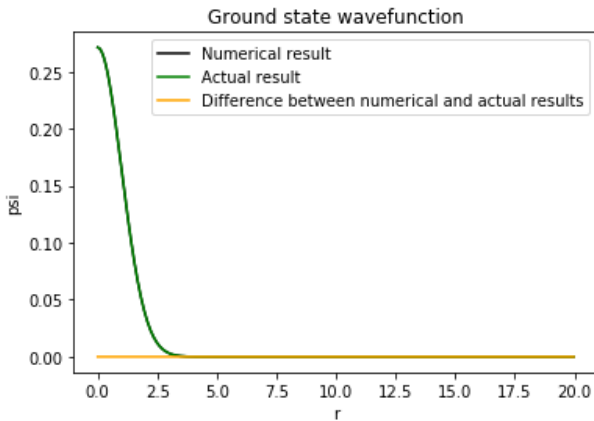
Figure 4: Ground state with 2D Hankel

We get an error of $\sim 0.0002\%$. Using the 2d fourier transform, we also achieve very accurate results.
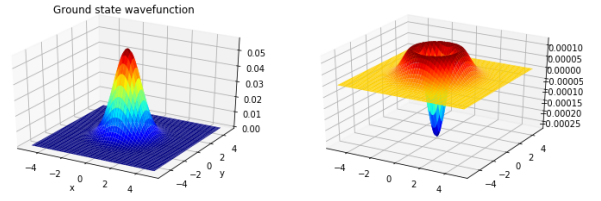
(a) Numerical 2D ground state wavefunction (b) Difference between numerical and actual solutions

Figure 5: 2D Ground state using Fourier transforms (Sorry the graphs are small)

An average error of $\sim 0.2\%$ is achieved.

Lastly, at certain values of γ and D, we expect the wavefunction have a bioconcave shape, like a red blood cell. This is shown clearly below.
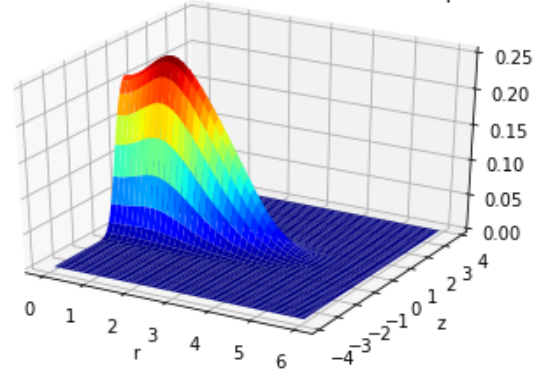
Figure 6: 3D plot of wavefunction using Hankel transform
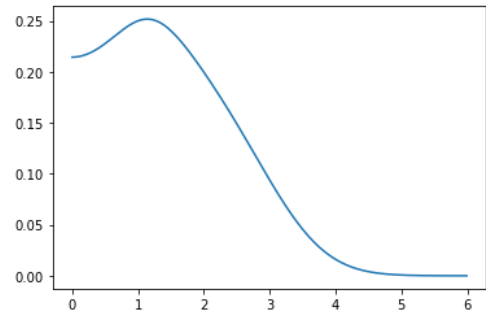

Figure 7: 1D slice of the above wavefunction along z=0.

8 Thomas Fermi

The Thomas Fermi radius for a given axis is given by

$$R_i = \sqrt{\frac{2\mu}{m\omega_i^2}}, \tag{8.1}$$

$$\mu = \frac{\hbar\bar{\omega}}{2}\left(\frac{Na}{x_s}\right)^{\frac{2}{5}}, \tag{8.2}$$

where ω_i is the harmonic frequency along that axis and μ is the chemical energy. DO CONTACT

9 Contact interactions

A good check for validity is whether our solutions agree with the analytical solution in the Thomas-Fermi regime. Firstly, we compare our Quasi 2D solution with the analytical solution and we see we achieve very high accuracy.
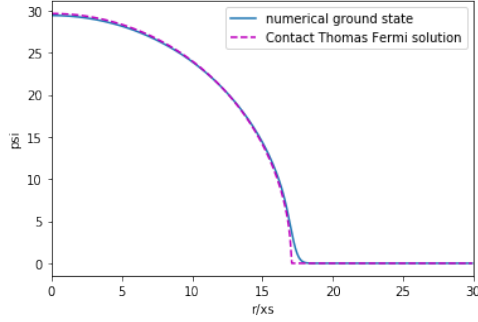

Figure 8: Thomas fermi regime with gamma = 50, N=4e5, using the Quasi 2D approach

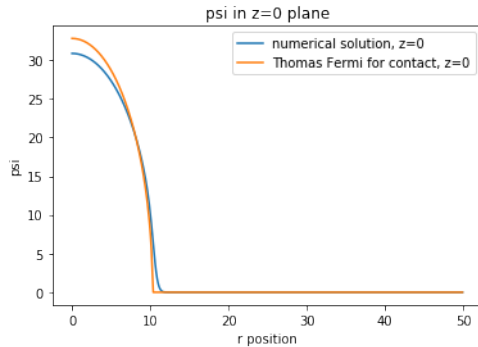We now compare our full 3D solution using the Hankel transform and the fast cosine transform,

Figure 9: Thomas fermi regime with gamma = 5, N=2e5, using the 3D Hankel approach

The discrepancies between the analytical solutions and our solutions may be due to the fact that the Thomas-Fermi solution is only valid up to the edges of the cloud, where the Thomas-Fermi approximation becomes discontinuous.

10 Purely dipolar interactions

The extension of the Thomas-Fermi analysis remains valid in a purely dipolar condensate with modified terms, and when the Quasi 2D approximation becomes valid this becomes especially simple. This is because the dipolar interaction can be rewritten as a short-range term and a long-range one Ref[1]. This is shown below for dipoles orientated along the z-axis:

$$U_{3D} = \frac{1 - 3\cos^2(\theta)}{|\mathbf{r}|^3} = -\frac{4\pi}{3}\delta(\mathbf{r}) - \frac{\partial^2}{\partial z^2}\left(\frac{1}{|\mathbf{r}|}\right) \quad (10.1)$$

In the limit of large D and γ this long-range term can be neglected aswell as the kinetic energy term, thus resulting in the dipolar TF regime.
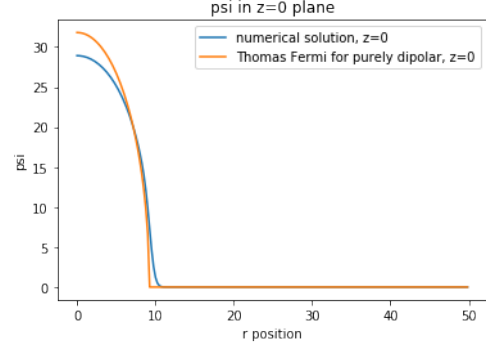

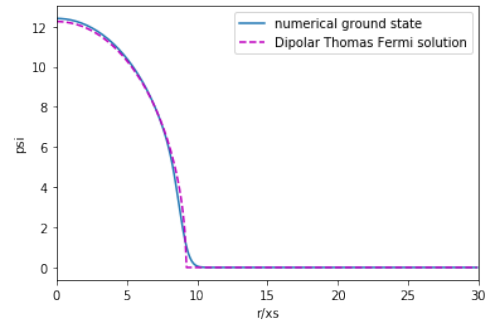Figure 10: Dipolar Thomas-fermi regime with gamma = 80, N=2e4, using the 3D Hankel approach

Figure 11: Dipolar-Thomas fermi regime with gamma = 5, N=2e5, using the Quasi 2D approach

11 Discussion of stability of a purely dipolar gas

11.1 In a harmonic trap

In general, the higher the trap ratio (λ), the more dipoles are required to make the condensate unstable. (This is due to fewer dipoles above or below any given dipole, since the dipole force is attractive in the cone above a dipole). Eventually, the BEC always becomes unstable for a large enough number of particles (for a given C_{dd}).

Figure 12 shows the stability using the 3D hankel approach. Black and white regions represent stable and unstable regimes respectively, and red represents the regime where biconcave (red blood cell) ground states are achieved. Figure 13 shows the same but using higher resolution, and unfortunately the colours are defined in the opposite way (obviously easily fixed). This shows strong agreement with fig[INSERT FIG NUMBER FROM RADIAL PAPER AND INSERT REFERENCE], showing the validity of our approach.
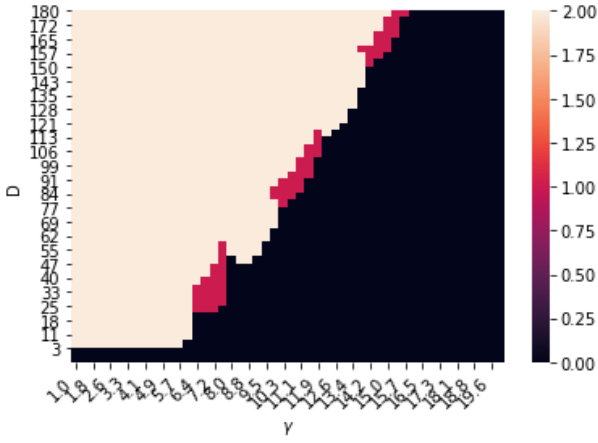
Figure 12: Stability plot of gamma against the dimensionless parameter D. The x axis is dipole strength and the y axis is gamma.
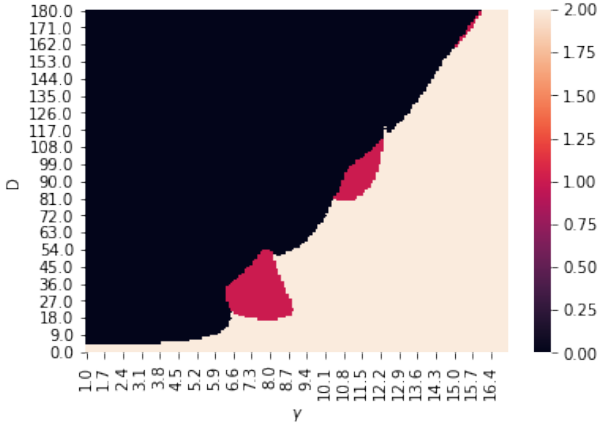

Figure 13: Stability plot of gamma against the dimensionless parameter D. The x axis is dipole strength and the y axis is gamma.

11.2 In a pancake trap

In a similar fashion to the harmonic trap, we define the dimensionless dipole interaction parameter, $D^{box} = \frac{mN\mu_0\bar{\mu}^2}{4\pi\hbar^2 L}$ where L is the length scale of the trap, normally defined to be the size of the trap in the r direction. We see that γ and D are different, and using equation (1.7), γ is now $\frac{mw_z L^2}{\hbar}$. Note now $\gamma \propto w_z$. To give an idea of the ranges of γ and D, we use a typical set of parameters shown below:

$$m = 2.78 \times 10^{-25}[kg], w_z = 20\pi - 100\pi[rad/s],$$
$$L = 1 \times 10^{-5}[m], N = 10^5, \bar{\mu} \approx 7\mu_B[J/T]$$

where μ_B is the Bohr magneton.

We get $\gamma = 16 - 82$ and $D_{box} = 104$.

However these numbers greatly depend on L, which is proportional to the trap size. Defining γ in this way is completely analogous to the harmonic case, as for both cases we define it as

$$\gamma = \frac{L^2}{l_z^2}. \tag{11.1}$$

where L and l_z are the length scales in the r and z direction respectively ($l_z = \sqrt{\frac{\hbar}{m\omega_z}}$). However, these don't equate to the same geometric situations. This is due to L representing a different fraction of the cloud size if it's defined to be the size of the trap. This means the ranges of gamma for the two cases which equate to roughly the same geometric ratios will be different. To get round this, we can define the box potential length scale to be a fraction of the box size, so when $\gamma = 1$ the height and width of the cloud will be approximately equal. This means that the ranges of gammas will equate to the same geometric ratios with this adjustment. Going into dimensionless units and setting the size of the box to be $3L$, we achieve the following graph.
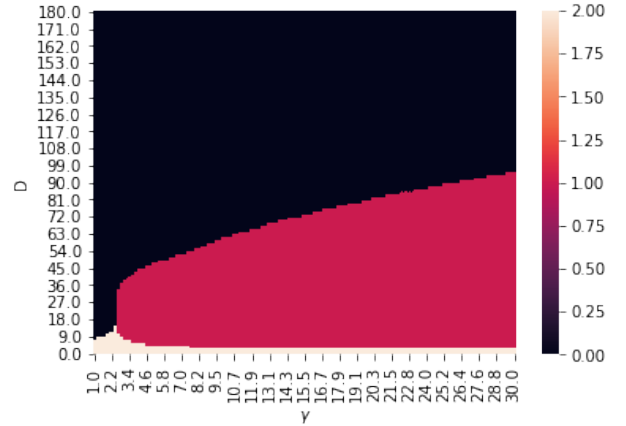

Figure 14: Stability plot of gamma against the dimensionless parameter D, with the size of the trap set to $3L$. White regions show stable areas. Red regions show stable areas, but with the maximum value of the wavefunction not at the centre. Black regions indicate instability.

This diagram shows for low D the maximum density still lies in the middle (show as white in the diagram), which is expected for D=0. As both D and gamma increase the maximum density lies at the outer regions of the cloud. This density oscillation is shown in Figure 15 [NEED TO INCLUDE THE VALUE OF D AND GAMMA FOR THIS PLOT].
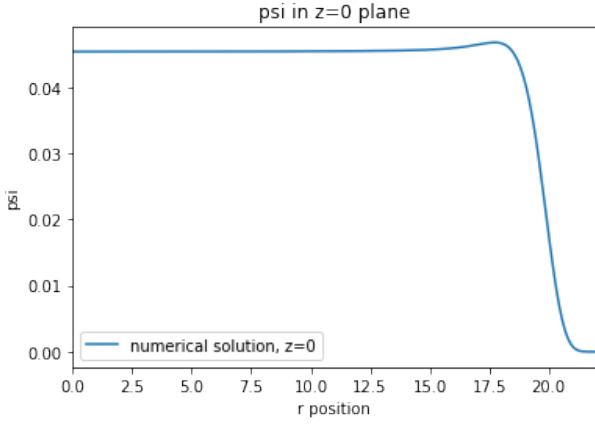
10

Figure 15: psi in the z=0 plane using a circular box potential, the maximum density is situated close to the edge of the cloud, where in this case $R_{box} = 20L$.
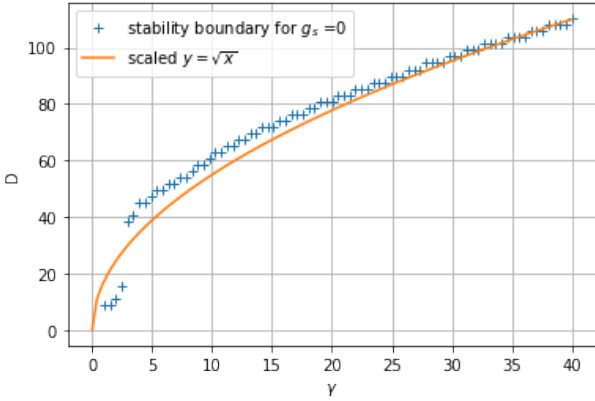

Figure 16: stability boundary for a purely dipolar gas, it appears that it's tending to Eq 11.2.

In [INSERT REFERENCE FOR NU PAPER] they predict for a gas unconfined in the r plane and harmonically confined in the z direction, that

$$\gamma \propto D^2 \tag{11.2}$$

on the stability boundary for a purely dipolar gas. This is shown from fig 5(b) IN REF [INSERT REFERENCE FOR NU PAPER] where it can be seen that for $g_s = 0$,

$$\frac{nC_{dd}}{3\hbar\omega_z l_z} = const. \tag{11.3}$$

From this (11.2) can be derived. It follows from this that as the size of our box increases, it would seem sensible for our stability plot to tend to (11.2). Figure 14 seems to show that this might be true for high gamma, but a more conclusive plot is definitely needed. There seems to be the opposite relationship for lower gamma, as can be shown by figure 16 which used $R_{box} = 20L$, but this may just be a problem with the code. Over the next week or so we should be able to get some better plots, these are really just giving a rough idea of what it looks like.
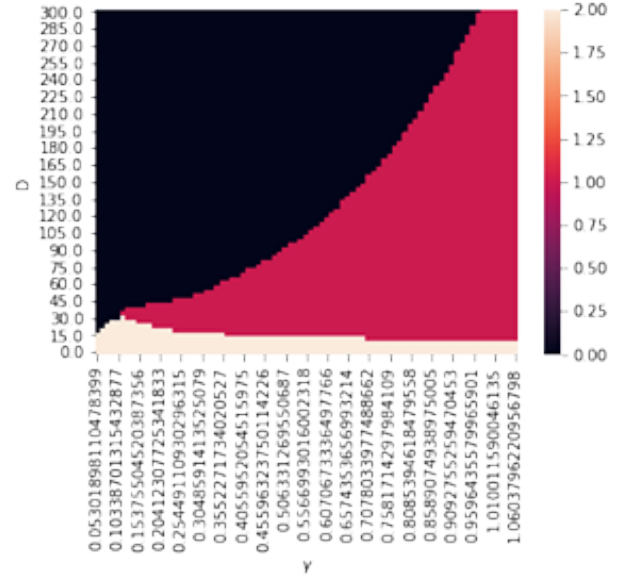

Figure 17: Stability plot of gamma against the dimensionless parameter D, with $R_{box} = 20L$. White regions show stable areas. Red regions show stable areas, but with the maximum value of the wavefunction not at the centre. Black regions indicate instability.

12 Stability outside the purely dipolar regime

We can also analyse the stability of the gas outside the purely dipolar regime. In [INSERT REFERENCE FOR NU PAPER] they determine two dimensionless parameters ν, ν_d, where if constant, the GPE is invariant. For our analysis we confine the dipoles to be aligned in the z direction which leads to the following,

$$\nu = \frac{n[3g + 2C_{dd}]}{3\hbar\omega_z l_z} \tag{12.1}$$

$$\nu_d = \frac{nC_{dd}}{3\hbar\omega_z l_z} \tag{12.2}$$

These are equavalent to equations (6) and (16) respectively in [INSERT REFERENCE FOR NU PAPER] with $\alpha = 0$. If we assume that the gas is uniform in the r direction we can rewrite them in our dimensionless variables. Obviously this is not true at the edge of the gas, but as the gas becomes larger in the r direction the edge becomes insignificant. With this assumption, i.e.

$$n = \frac{N}{\pi(\Omega L)^2} \tag{12.3}$$

we get the following expressions:

$$\nu = \frac{(3g_s + 8\pi D)l_z}{3\pi L\Omega^2} \tag{12.4}$$

$$\nu_d = \frac{4Dl_z}{3L\Omega^2} \tag{12.5}$$

For $\gamma = 100$ we achieve good agreement with the unconfined case.
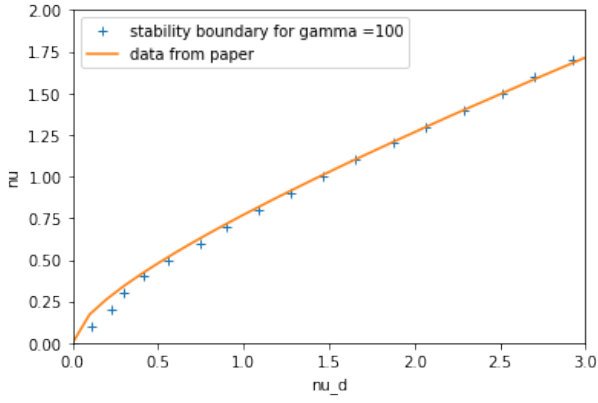
Figure 18: stability boundary, where for any ν_d above the boundary, the BEC becomes unstable. We see our results are in good agreement with the unconfined case, The labels are the wrong way round, nu should be the x axis.
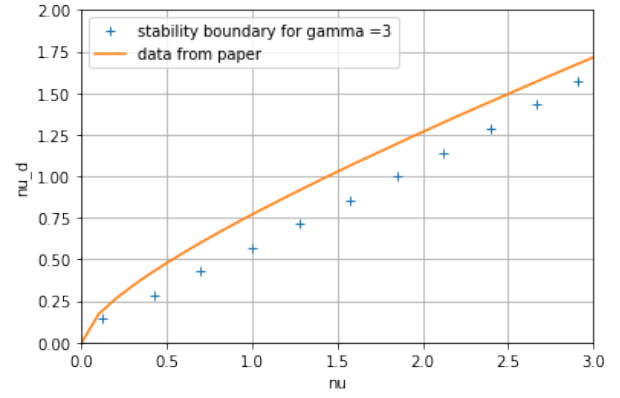

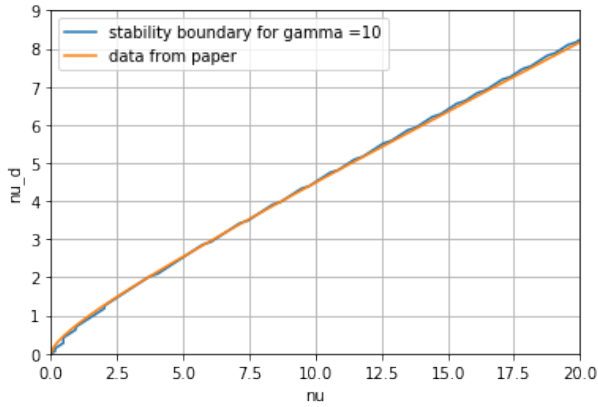Figure 20: We see that the unconfined approximation starts to break down at very low gamma.

None of these plots are conclusive, and they all deviate from the unconfined case at low ν, and potentially for very high ν also. To have a better comparison we should have plots all with the same range which is easily done.

13   Issues

One issue we seem to be getting is that the code doesn't work for very high γ. One reason is my idea that the time scale was independent of γ may be incorrect, as by dividing dt by γ seems to give more sensible results at very high γ. However this does increase computational time due to more iterations being needed for convergence with low dt. But even accounting for this, there still seems to be issues for very high γ. My guess at the moment is a floating point precision error, as for some calculations we are using variables that are proportional to γ^2 along with variables that are not. This may lead to a loss of information. This is the main justification for having the length scale be a fraction of the box size rather than the box size itself, as lower gammas are needed to achieve the same geometric situations. It seems strange that a precision error would lead to large differences, but I can't see any other reason for this and the code clearly works very well for sensible ranges of γ.

Figure 19: We see that the unconfined approximation seems to hold for gamma =10.

For very low γ the stability boundary starts to deviate from the unconfined case and it seems it decrease in stability for a given ν.

References

[1] Weizhu Bao and Yongyong Cai. Mathematical theory and numerical methods for bose-einstein condensation. *Kinetic & Related Models*, 6(1):1–135, 2013.

[2] Luigi Galati. Numerical solutions to the gross-pitaevskii equation for bose-einstein condensates. Master's thesis, Georgia Southern University, 2013.

[3] Armen Oganesov. *Modeling the Gross-Pitaevskii Equation Using the Quantum Lattice Gas Method.* PhD thesis, 2018. Copyright - Database copyright ProQuest LLC; ProQuest does not claim copyright in the individual underlying works; Last updated - 2020-01-27.

[4] Thomas Bland. *Elementary and topological excitations in ultracold dipolar Bose gases*. PhD thesis, Newcastle University, 2018.

[5] Shai Ronen, Daniele C. E. Bortolotti, and John L. Bohn. Bogoliubov modes of a dipolar condensate in a cylindrical trap. *Physical Review A*, 74(1), Jul 2006.

[6] You Kai-Ming, Wen Shuang-Chun, Chen Lie-Zun, Wang You-Wen, and Hu Yong-Hua. A quasi-discrete hankel transform for nonlinear beam propagation. *Chinese Physics B*, 18(9):3893–3899, sep 2009.

[7] M. L. Chiofalo, S. Succi, and M. P. Tosi. Ground state of trapped interacting bose-einstein condensates by an explicit imaginary-time algorithm. *Phys. Rev. E*, 62:7438–7444, Nov 2000.

[8] Q. Zhang and M. I. Hayee. Symmetrized split-step fourier scheme to control global simulation accuracy in fiber-optic communication systems. *Journal of Lightwave Technology*, 26(2):302–316, 2008.

[9] Thiab R Taha and Mark I Ablowitz. Analytical and numerical aspects of certain nonlinear evolution equations. iii. numerical, korteweg-de vries equation. *Journal of Computational Physics*, 55(2):231 – 253, 1984.

[10] Xueming Liu. Adaptive higher-order split-step fourier algorithm for simulating lightwave propagation in optical fiber. *Optics Communications*, 282(7):1435 – 1439, 2009.

[11] R. Kishor Kumar, Luis E. Young-S., Dušan Vudragović, Antun Balaž, Paulsamy Muruganandam, and S.K. Adhikari. Fortran and c programs for the time-dependent dipolar gross–pitaevskii equation in an anisotropic trap. *Computer Physics Communications*, 195:117 – 128, 2015.